

Distortion of the perfect lattice structure in bilayer graphene

Vitor M. Pereira

Department of Physics, Boston University, 590 Commonwealth Avenue, Boston, MA 02215, USA

R. M. Ribeiro

Center of Physics and Department of Physics, University of Minho, P-4710-057, Braga, Portugal

N. M. R. Peres

Center of Physics and Department of Physics, University of Minho, P-4710-057, Braga, Portugal

A. H. Castro Neto

Department of Physics, Boston University, 590 Commonwealth Avenue, Boston, MA 02215, USA

(Dated: November 21, 2018)

We consider the instability of bilayer graphene with respect to a distorted configuration in the same spirit as the model introduced by Su, Schrieffer and Heeger. By computing the total energy of a distorted bilayer, we conclude that the ground state of the system favors a finite distortion. We explore how the equilibrium configuration changes with carrier density and an applied potential difference between the two layers.

PACS numbers: 81.05.Uw

I. INTRODUCTION

A planar arrangement of carbon atoms covalently bound via sp^2 orbitals exhibits a honeycomb structure and is denoted graphene. Graphene rose rapidly to the forefront of research in condensed matter physics, mostly because of the peculiar electronic structure that emerges from its crystal structure, and the consequent wealth of rich and unexpected phenomena¹. Seminal experiments on two dimensional crystals established graphene as an accessible reality², and immediately unveiled numerous surprises, both on a fundamental level – like a new form of quantized Hall effect – and on a practical and technological level – like the highly efficient field effect and high electronic mobility^{3,4}. Most of the appealing phenomenology of graphene owes to the fact that electron dynamics in this system can be described in terms of chiral massless Dirac fermions³ and, in fact, graphene does exhibit many properties characteristic of relativistic particles^{5,6}.

Equally remarkable phenomena occur in bilayer graphene, which consists of two adjacent graphene planes stacked in the A-B fashion typical of graphite. Bilayer graphene displays the same sample quality and quasi-ballistic transport characteristic of its single layer counterpart⁷, but brings also its share of new physics stemming from the nature of its charge carriers: chiral massive electrons⁸. Most interesting is the fact that, although gapless in its pristine form, a potential difference between the two layers opens a gap in the spectrum that can be controlled via chemical doping⁹ or gating^{10,11,12}.

Despite such favorable prospects, the amount of knowledge gathered in the context of bilayer graphene still lags behind the intensity committed to single layer graphene. In this brief paper, we address a particular aspect of the electron-phonon interaction in bilayer graphene, namely

the tendency to relax the perfect crystal structure and generate a static, uniform deformation. This effect is inspired, and similar in spirit, to the well known Peierls instability that occurs in polyacetylene chains. As shown by Su, Schrieffer and Heeger (SSH)^{13,14}, in polyacetylene the one dimensional chain of carbon atoms has a half-filled electronic ground state that is unstable with respect to a spontaneous dimerization. This dimerization opens a sizeable gap in the spectrum that can be easily detected experimentally¹⁵.

The instability we envisage for bilayer graphene is related with the application of SSH's ansatz to the inter-

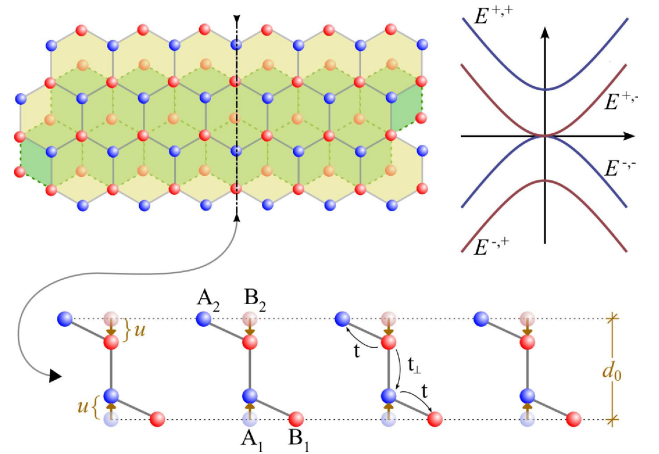


FIG. 1: (color online) Transverse view (bottom) along the dashed-dotted line (top left) of the lattice distortion considered in the text. The vertical displacement of the carbon atoms connected by the hopping integral t_{\perp} is represented by the parameter u . In the top right we schematically represent the bandstructure in the vicinity of the Dirac point.

plane hopping, t_{\perp} . From the outset, the atoms lying in the A and B sublattices within each layer are not equivalent, since only one of the sublattices connects to the adjacent plane (Fig. 1). This has important experimental consequences: one example is the known fact that in tunneling experiments one typically detects only one of the sublattices of the topmost layer¹⁶. In the absence of a potential difference between the two layers (unbiased situation), the bilayer is a zero gap semiconductor, with hyperbolic bands touching at the Fermi energy. A change in the interlayer hopping will not change this situation, and thus the gap can still be tuned through the potential difference between layers. However, as shown below, the electron-phonon interaction might indeed lead to a stable distorted configuration.

II. THE MODEL

A. Tight binding description of a biased bilayer

The electronic Hamiltonian of a biased bilayer consists of two contributions, $H_e = H_{tb} + H_V$, where H_{tb} is the tight-binding Hamiltonian for the graphene bilayer, and H_V reflects the electrostatic bias applied between the two graphene planes. The tight-binding Hamiltonian H_{tb} contains in itself three terms describing electron itinerancy among each individual plane and between the two planes. In detail we have

$$H_{tb} = H_{tb1} + H_{tb2} + H_{\perp}, \quad (1)$$

with

$$H_{tb1} = -t \sum_{\mathbf{R}, \sigma} [a_{1\sigma}^{\dagger}(\mathbf{R}) b_{1\sigma}(\mathbf{R}) + a_{1\sigma}^{\dagger}(\mathbf{R}) b_{1\sigma}(\mathbf{R} - \mathbf{a}_1) + a_{1\sigma}^{\dagger}(\mathbf{R}) b_{1\sigma}(\mathbf{R} - \mathbf{a}_2) + \text{H.c.}], \quad (2)$$

$$H_{tb2} = -t \sum_{\mathbf{R}, \sigma} [a_{2\sigma}^{\dagger}(\mathbf{R}) b_{2\sigma}(\mathbf{R}) + a_{2\sigma}^{\dagger}(\mathbf{R} + \mathbf{a}_1) b_{2\sigma}(\mathbf{R}) + a_{2\sigma}^{\dagger}(\mathbf{R} + \mathbf{a}_2) b_{2\sigma}(\mathbf{R}) + \text{H.c.}], \quad (3)$$

$$H_{\perp} = -t_{\perp} \sum_{\mathbf{R}, \sigma} [a_{1\sigma}^{\dagger}(\mathbf{R}) b_{2\sigma}(\mathbf{R}) + b_{2\sigma}^{\dagger}(\mathbf{R}) a_{1\sigma}(\mathbf{R})], \quad (4)$$

and

$$H_V = \frac{V}{2} \sum_{\mathbf{R}, \sigma} [a_{1\sigma}^{\dagger}(\mathbf{R}) a_{1\sigma}(\mathbf{R}) + b_{1\sigma}^{\dagger}(\mathbf{R}) b_{1\sigma}(\mathbf{R})] - \frac{V}{2} \sum_{\mathbf{R}, \sigma} [a_{2\sigma}^{\dagger}(\mathbf{R}) a_{2\sigma}(\mathbf{R}) + b_{2\sigma}^{\dagger}(\mathbf{R}) b_{2\sigma}(\mathbf{R})]. \quad (5)$$

In the above equations \mathbf{a}_1 and \mathbf{a}_2 represent the elementary translations of the honeycomb lattice. In the presence of an electrostatic bias V , the electronic dispersion is given by the four branches

$$E_{\mathbf{k}}^{\pm, \pm} = \pm \frac{1}{2} \sqrt{2t_{\perp}^2 + V^2 + 4t^2 |\phi_{\mathbf{k}}|^2} \pm \Delta_{\mathbf{k}}, \quad (6)$$

where

$$\Delta_{\mathbf{k}} = 2\sqrt{t_{\perp}^4 + 4t^2(t_{\perp}^2 + V^2)|\phi_{\mathbf{k}}|^2}. \quad (7)$$

When $V = 0$ Eq. (6) simplifies to

$$E_{\mathbf{k}}^{\pm, \pm} = \pm \frac{1}{2} \left(\pm t_{\perp} + \sqrt{t_{\perp}^2 + 4t^2 |\phi_{\mathbf{k}}|^2} \right), \quad (8)$$

where $\phi_{\mathbf{k}}$ is associated with the dispersion of a single layer, and is given by

$$\phi_{\mathbf{k}} = 1 + e^{i\mathbf{k} \cdot \mathbf{a}_1} + e^{i\mathbf{k} \cdot \mathbf{a}_2}. \quad (9)$$

In order to proceed analytically, we approximate $|\phi_{\mathbf{k}}|$ by

$$|\phi_{\mathbf{k}}| \simeq \frac{3}{2} a q, \quad (10)$$

where we took $\mathbf{k} = \mathbf{K} + \mathbf{q}$ to be close to the Dirac point in the honeycomb Brillouin zone, and amounts to using the effective mass approximation for bilayer graphene (a is the carbon-carbon distance).

B. Parametrization of Distortion

We consider a distortion of the perfect lattice structure of the bilayer, such that the A and the B atoms, connected by the hopping parameter t_{\perp} , distort along the vertical direction by an amount u_i (Fig. 1). In the spirit of the SSH model for polyacetylene¹⁴ we assume that, to leading order in the strain, the effect of this distortion is to change the value of t_{\perp} according to

$$t_{\perp} = t_{\perp}^0 (1 + \alpha u_i), \quad (11)$$

where t_{\perp}^0 is the value of the interlayer hopping of the undistorted lattice. For small u_i , the in-plane hopping t is affected by this distortion only at higher orders in u_i , and therefore we neglect its variation. This distortion will naturally induce an elastic restoring force that we parametrize through the term

$$H_{el} = K \sum_{i=1}^{N_c} u_i^2 + \sum_{i=1}^{N_c} \frac{P_i^2}{M}, \quad (12)$$

N_c denoting the number of unit cells. In the static and homogeneous situation the kinetic term gives an average

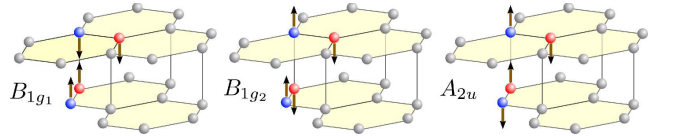


FIG. 2: (color online) Phonon modes along the c -axis in graphite, using the notation of Ref. 17. The modes A_{2u} and B_{1g2} are nearly degenerate at the center of the Brillouin zone, with $\omega \simeq 870 \text{ cm}^{-1}$ ^{17,18}.

null contribution and all u_i acquire the same mean value: $u_i = u$. This leads to a total elastic energy that reads:

$$E_{\text{el}} = K \sum_{i=1}^{N_c} u^2 = N_c u^2. \quad (13)$$

The stability analysis of such a distorted phase proceeds by minimization of the total electronic and elastic energy, given by $H_e + H_{\text{el}}$, with respect to the distortion u . We underline that, unlike in the original polyacetylene model¹⁴, the parametrization (11) does not change the original periodicity of the lattice, and therefore does not require a density commensurability.

C. Estimation of parameters

A precise estimation of the parameters required for the computation of the stable distorted configuration is not easy nor unique. On the one hand, little is known with respect to the structural and elastic properties of a graphene bilayer, and thus we will rely on the corresponding knowledge that exists for graphite. On the other hand, details like the type of substrate, can significantly alter these parameters, as happens, for instance with the phonon spectrum that can be sensitive to substrate and other constraints in the system.

We will therefore resort to the structural parameters (lattice constant and elastic coefficients) known for A-B stacked graphite. The carbon-carbon distance is $a \simeq 1.42 \text{ \AA}$, and the graphene unit cell has an area given by $A_c = 3\sqrt{3}a^2/2$. The equilibrium interlayer distance is given by $d_0 = c_0/2 \simeq 3.35 \text{ \AA}$, and corresponds to half the unit cell height of A-B stacked graphite^{19,20,21}.

The value of the stiffness, K , can be estimated from the phonon spectrum of graphite. In particular the B_{1g_2} optical (out-of-plane) phonon mode has a frequency of $\omega \approx 870 \text{ cm}^{-1}$, which is seen both experimentally²², and from ab-initio calculations¹⁸. As a result of the weak interlayer interaction, this phonon is essentially degenerate with the out-of-plane phonon A_{2u} present in a single layer of graphene. These normal modes are represented in Fig. 2. We can assume that K relates to this frequency through $Ka^2 \sim m\omega^2 a^2/4$, where m is the carbon atom mass, and $a \simeq 1.42 \text{ \AA}$ is the carbon-carbon distance²³. As a result we obtain as estimate for the stiffness $K \simeq 8.5 \text{ eV} \cdot \text{\AA}^{-2}$.

With respect to the electron-phonon coupling α , its estimation is most straightforward from the knowledge of how the interplane hopping varies with distance. The interplane hopping, t_{\perp} corresponds to the tight-binding parameter $V_{pp\sigma}$ in the two center Slater-Koster formalism^{24,25}. For instance, assuming that

$$V_{pp\sigma}(r) \simeq Ae^{-\alpha r} \quad (14)$$

one can extract α from interpolation of the hoppings γ_1 the in-plane $V_{pp\sigma}(a)$ for graphite. Using the values^{17,26}

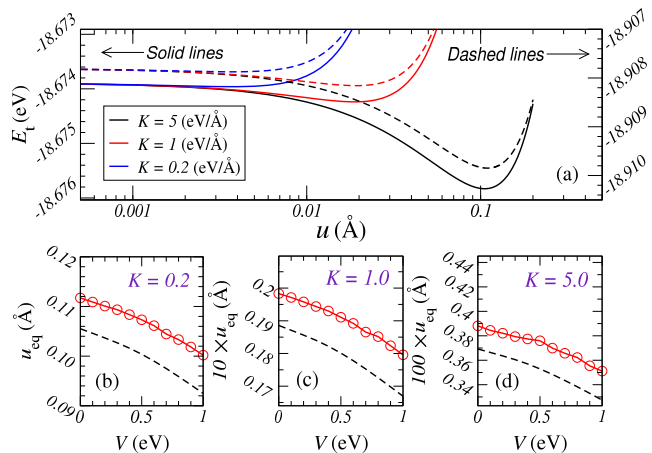


FIG. 3: (color online) (a) Total energy E_t per unit cell as a function of the deformation parameter u , and for different values of K . The left (right) vertical axis pertains to the solid (dashed) curves. (b-d) The equilibrium radius as a function of the bias voltage, V . In all panels dashed lines refer to the Dirac approximation, whereas full lines have been calculated using the full tight-binding dispersion in Eq. (6). Notice that in panels (c) and (d) the vertical axis is amplified 10 and 100 times, respectively. Other parameters used are $t_{\perp}^0 = 0.3 \text{ eV}$, $t = 3.0 \text{ eV}$, $\alpha = 1.5 \text{ \AA}^{-1}$.

$\gamma_1 \approx 0.4 \text{ eV}$ and $V_{pp\sigma}(a) \approx 3.7 \text{ eV}$ we obtain $\alpha \approx 1.2 \text{ \AA}^{-1}$. Alternatively to the formula (14), one could use a more refined interpolation formula for $V_{pp\sigma}(r)$ as discussed in Ref. 27. This yields $\alpha \approx 1.8 \text{ \AA}^{-1}$, consistent with the previous estimate.

Finally, several recent experiments on the bilayer^{28,29,30} show that the value of t_{\perp}^0 is essentially the value expected in graphite, $t_{\perp}^0 \approx 0.3 \text{ eV}$, the same applying to the in-plane hopping, $t \approx 3 \text{ eV}$.

III. AB-INITIO CALCULATION OF THE ELASTIC CONSTANT

In addition to the above estimates of the model parameters, we have extracted the compression elastic constant from a first principles calculation. Density functional calculations in graphite and related compounds must be carried with caution for it is known that different implementations of density functional theory can yield noticeably different results^{18,31}. Having this in mind, we calculated the equilibrium distance between graphene planes in the bilayer by resorting to two different approximations: the Generalized Gradient Approximation (GGA) and the Local Density Approximation (LDA).

GGA — We sampled the BZ according to the scheme proposed by Monkhorst-Pack³², with a grid of $12 \times 12 \times 4$ \mathbf{k} -points. Bilayer graphene was modeled in a slab geometry by including a vacuum region in a supercell containing 4 carbon atoms (2 for each graphene sheet). In

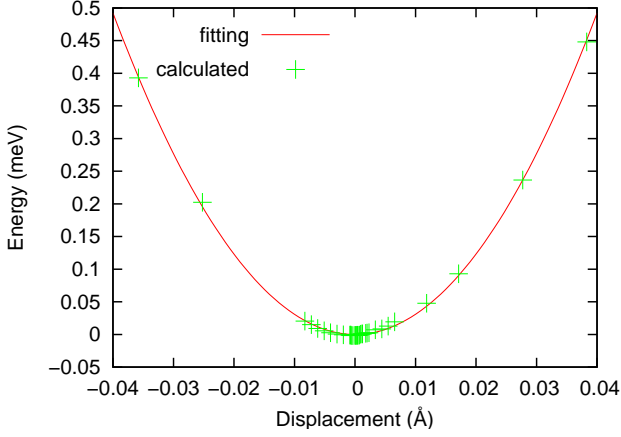


FIG. 4: Energy as a function of distance between layers measured with respect to the equilibrium position, and calculated within the GGA. The positive direction indicates a displacement towards the other graphene sheet. The zero value energy is the energy of the fully relaxed sample.

the normal direction (z -direction), the vacuum separating repeating slabs has more than 10 Å, and the size of the supercell in the z -direction was optimized to make sure there was no interaction between repeating slabs.

LDA — In this case the BZ was sampled within the same scheme with a grid of $4 \times 4 \times 1$ \mathbf{k} -points, and using a supercell comprising 8 carbon atoms (4 for each sheet). Adjacent slabs along the z direction were separated by more than 30 Å, and the size of the supercell along this direction was again optimized.

In either case an increase in the number of sampling points did not result in a significant total energy change, and the vertical separation quoted above guarantees the absence of interaction between adjacent slabs. We used dual-space separable pseudopotentials by Hartwigsen, Goedecker, and Hutter³³ to describe the ion cores. In a first step, all the atoms were fully relaxed to their equilibrium positions. Then one of the graphene sheets was moved as a whole in the z -direction by very small displacements, and the total energy of the system was calculated, without any further relaxation.

Figure 4 shows the GGA variation of the total energy relative to the relaxed sample, as a function of the displacement from the equilibrium position. Also shown is the parabola that was fitted to the calculated values. The fitting gave a value of $K = 0.615 \pm 0.002$ eV/Å², per unit cell. The same calculation within LDA yields $K = 4.15 \pm 0.06$ eV/Å². The two calculations therefore differ by one order of magnitude, signaling the fact that, like other systems derived from graphite, density functional calculations are very sensitive to the details of the approximation used.

IV. TOTAL ENERGY AT CONSTANT μ

Our main objective is to quantify the equilibrium distortion that is expected to emerge from the competition between elastic and electronic energies in the ground state. For illustration purposes we consider first the computation of the total energy in the (potentially artificial) case where the chemical potential is held constant. In particular, we assume that the density of carriers in the bilayer is such that the chemical potential is located between $E_{q=0}^{+,+}$ and $E_{q=0}^{+,-}$:

$$\mu = \frac{V + \sqrt{V^2 + 4t_{\perp}^2}}{4}. \quad (15)$$

Let us start with an unbiased bilayer ($V = 0$). In this case the total electronic energy per unit cell is given by

$$\frac{E_e}{N_c} = \frac{gA_c}{2\pi} \int_0^{q_c} q dq (E_q^{-,+} + E_q^{-,-}) + \frac{gA_c}{2\pi} \int_0^{q_F} q dq E_q^{+,-}. \quad (16)$$

The integral is elementary leading to

$$\begin{aligned} \frac{E_e}{N_c} = & \frac{gA_c}{2\pi} t_{\perp} \left(\frac{q_t^2}{6} - \frac{q_F^2}{4} \right) - \frac{gA_c}{6\pi} t_{\perp} q_t^2 \left[1 + \left(\frac{q_c}{q_t} \right)^2 \right]^{3/2} \\ & + \frac{gA_c}{12\pi} t_{\perp} q_t^2 \left[1 + \left(\frac{q_F}{q_t} \right)^2 \right]^{3/2}, \end{aligned} \quad (17)$$

where the momenta q_F , q_c and q_t are defined as

$$q_t = \frac{t_{\perp}}{3ta}, \quad q_c = \sqrt{\frac{2\pi}{A_c}}, \quad q_F = \frac{\sqrt{(2\mu + t_{\perp})^2 - t_{\perp}^2}}{3ta}, \quad (18)$$

and $A_c = 3\sqrt{3}a^2/2$ is the area of the graphene unit cell. The total energy E_t per unit cell is given by

$$\frac{E_t}{N_c} = \frac{E_e}{N_c} + Ku^2. \quad (19)$$

These two terms compete in such a way that the minimum energy state is achieved for a finite value of u .

The dashed lines of the top panels of Fig. 3 represent the total energy, E_t , as a function of the deformation u , using different values of the stiffness parameter, K . It is also instructive to investigate to what extent the approximation (10) influences the equilibrium deformations and, for that, we have performed the calculation of the total energies using the full tight-binding dispersions of Eq. (6). The results so obtained are represented in the same figure by the solid lines. It is clear from Fig. 3(a), that, besides yielding slightly larger absolute values for the energy, the full dispersion increases the equilibrium deformation by about 5 to 10%.

The analytical calculation in the presence of a finite bias ($V \neq 0$), is also straightforward. The total energy is still given by Eq. (16), where $E_{\mathbf{k}}^{\pm,\pm}$ is now given by (6). The energy integrals are given in the appendix, the final

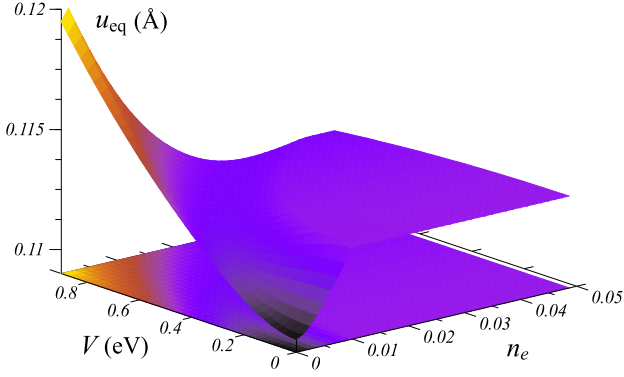


FIG. 5: (color online) Equilibrium deformation, u_{eq} , as a function of the electron density per unit cell (n_e) and the bias voltage (V). The parameters used are $t_{\perp}^0 = 0.3$ eV, $t = 3.0$ eV, $K = 0.2$ eV.Å⁻² and $\alpha = 1.5$ Å⁻¹.

result being

$$\frac{E_{el}}{N_c} = \frac{gA_c}{2\pi} \left[F^{-,+}(k) \Big|_0^{q_c} + F^{-,-}(k) \Big|_0^{q_c} + F^{+,-}(k) \Big|_0^{q_F} \right]. \quad (20)$$

The primitives $F^{\eta_1, \eta_2}(k)$ are calculated in the appendix, with the final result

$$F^{\eta_1, \eta_2}(k) = \frac{\eta_1}{8\nu_F^2(t_{\perp}^2 + V^2)} \left\{ \frac{R^{3/2}}{3\gamma} - \frac{\gamma x + \eta_2}{2\gamma^2} \eta_2 \sqrt{R} - \frac{\eta_2 \Delta}{8\gamma^{5/2}} \log(2\sqrt{\gamma R} + 2\gamma x + 2\eta_2) \right\}, \quad (21)$$

and the remaining parameters are defined in (B5).

Placing the chemical potential again at the midpoint between the two conduction bands at $q = 0$,

$$\mu = (V + \sqrt{4t_{\perp}^2 + V^2})/4, \quad (22)$$

the corresponding Fermi wavevector is

$$q_F = \frac{1}{2\nu_F} \sqrt{V^2 + 4\mu + 2\sqrt{4\mu(t_{\perp}^2 + V^2) - t_{\perp}^2 V^2}}, \quad (23)$$

and we obtain the results shown in the lower panel of Fig. 3 for the equilibrium radius. When V varies between 0 and 1 eV, the equilibrium radius shows a relative variation of $\sim 15\%$. In addition, it can be seen that the difference between using the Dirac approximation and the full tight-binding dispersion is, in accordance with the above, essentially a systematic increase in the equilibrium radius. For this reason, henceforth we will restrict the discussion to the results obtained within the Dirac approximation.

V. TOTAL ENERGY AT CONSTANT n_e

We consider now the more relevant case of a bilayer with constant carrier density, which can be tuned, for

instance, through a gate voltage. We define n_e as the number of electrons per unit cell, with respect to the charge-neutral situation in which the valence bands are fully occupied. In addition we will be concerned with electron doping only. The calculation of the electronic energy in this case requires, in general, the consideration of three distinct possibilities. Assuming a biased situation, and with respect to the notation defined in Fig. 7, we can have:

- (i) the Fermi level lying between E_1 and E_2 , in which case the Fermi surface consists of a Fermi ring characterized by two Fermi momenta $q_F^{III,1}$ and $q_F^{III,2}$, and the phase space exhibits a central hollow;
- (ii) the Fermi level lying between E_2 and E_3 , where we have a more conventional Fermi surface;
- (iii) the Fermi level lying above the bottom of the uppermost band, in which case we have again two Fermi momenta, q_F^{III} and q_F^{IV} , but the phase space is now simply connected.

The boundaries of these regimes can be easily identified through the two threshold densities

$$n_e^* = \frac{gA_c}{4\pi} q_2^2, \quad \text{and} \quad n_e^{**} = \frac{gA_c}{4\pi} q_3^2. \quad (24)$$

It follows that the total electronic energy is computed as

$$\frac{E_e}{N_c} = \frac{gA_c}{2\pi} \int_0^{q_c} q dq (E_q^{-,+} + E_q^{-,-}) + \frac{gA_c}{2\pi} \int_{q_F^{III,1}}^{q_F^{III,2}} q dq E_q^{+,-} + \frac{gA_c}{2\pi} \int_0^{q_F^{IV}} q dq E_q^{+,+}, \quad (25)$$

where the integration limits of the last two terms are given by (see also Fig. 7 for notation)

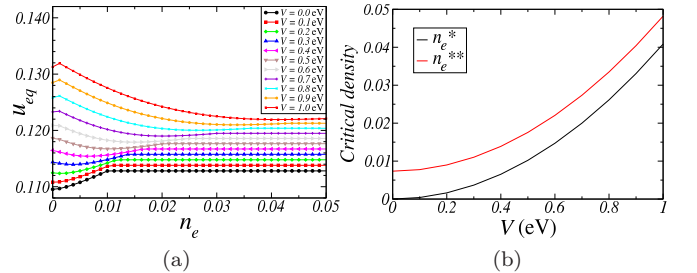


FIG. 6: (color online) (a) Selected cuts from Fig. 5 at constant bias V . For clarity, successive curves have been shifted vertically by 0.001 in the order of increasing V . (b) The densities n_e^* and n_e^{**} defined in Eq. (24), plotted as a function of V for the same parameters used in Fig. 5.

$$n_e < n_e^* : \quad (26a)$$

$$\begin{aligned} q_F^{IV} &= 0, \\ \begin{cases} n_e = \frac{gA_c}{4\pi} \left((q_F^{III,2})^2 - (q_F^{III,1})^2 \right) \\ 2\nu_F^2 (q_F^{III,1})^2 - \sqrt{t_\perp^4 + 4\nu_F^2 (q_F^{III,1})^2 (t_\perp^2 + V^2)} = 2\nu_F^2 (q_F^{III,2})^2 - \sqrt{t_\perp^4 + 4\nu_F^2 (q_F^{III,2})^2 (t_\perp^2 + V^2)} \end{cases} \end{aligned} \quad (26b)$$

$$n_e^* < n_e < n_e^{**} : \quad (26c)$$

$$\begin{aligned} q_F^{IV} &= 0, \\ q_F^{III,1} &= 0, \\ q_F^{III,2} &= \frac{gA_c}{4\pi} \left(\frac{1}{n_e} \right)^{-1/2}. \end{aligned} \quad (26c)$$

$$n_e > n_e^{**} : \quad (26c)$$

$$\begin{aligned} q_F^{III,1} &= 0, \\ \begin{cases} n_e = \frac{gA_c}{4\pi} \left((q_F^{III,2})^2 + (q_F^{IV})^2 \right) \\ 2\nu_F^2 (q_F^{III,2})^2 + \sqrt{t_\perp^4 + 4\nu_F^2 (q_F^{III,2})^2 (t_\perp^2 + V^2)} = 2\nu_F^2 (q_F^{IV})^2 - \sqrt{t_\perp^4 + 4\nu_F^2 (q_F^{IV})^2 (t_\perp^2 + V^2)} \end{cases} \end{aligned}$$

Minimizing the total energy with respect to u yields the equilibrium displacements plotted in Fig. 5, for different electron densities and bias voltages. The typical deformations for the parameters quoted in the figure are ~ 0.11 Å, which represents $\sim 8\%$ of the carbon-carbon distance, a . The variation of u_{eq} with n_e and V is non-monotonic. In particular, one notices that, for constant V , the equilibrium deformation tends to saturate beyond a given density. This can be appreciated in more detail in Fig. 6(a), where we present selected cuts of the same surface. The saturation can be understood from the interplay of two factors: on the one hand, the variation of V and n_e induce changes in the bandstructure only in a region close to the neutrality point; on the other hand, for high enough density, the Fermi level will always be considerably above the bottom of the uppermost band (E_3 in Fig. 7). In fact, comparing the values of n_e^* and n_e^{**} presented in Fig. 6(b), one can verify that the first sets the scale for the minimum in the curves of u_{eq} versus n_s , therefore defining the shape of the valley in the plot of Fig. 5. The value n_e^{**} , on the other hand, marks the onset of saturation.

VI. DISCUSSION AND CONCLUSIONS

We have shown that a graphene bilayer with A-B stacking can be unstable with respect to a Peierls-like distortion affecting the interplane bonds. This distortion preserves the bandstructure of the system, in the sense that, unlike the original Peierls problem, it does not lead to a gap in the unbiased case, nor to its closing in the bi-

ased situation. In addition, it was found that the general effect of the bias voltage is to increase the equilibrium deformation.

By comparing the results obtained with the full tight-binding dispersion of bilayer graphene with the effective mass approximation [Fig. 3(c-e)], we concluded that the former does not introduce significant changes in the equilibrium results, and therefore the low energy approximation is adequate to study this instability.

For the values of K used in Fig. 5, the magnitude of the deformation corresponds to roughly 10% of the in-plane carbon-carbon distance, and is significant. However, at this point one can hardly be definite about a specific value of the equilibrium deformation on account of the uncertainties in the estimation of the parameters K and α . The value used for K is close to the compressive stiffness found with the GGA calculation described above. But clearly, had we used the estimate for the phonon B_{1g2} (or the LDA result) instead, we would have obtained much smaller values of u_{eq} , as can be inferred from Fig. 3(d), although the qualitative features of Fig. 5 would be preserved. Hence a definitive conclusion as to the magnitude of the effect is deferred until the relevant parameters in bilayer graphene are experimentally available.

In the consideration of the electronic energy, we have accounted only for nearest neighbor in-plane and interplane hoppings. Additional hopping terms, like next-nearest neighbor and other interplane hoppings, should not change the qualitative picture presented here. On a quantitative level, even the ones that are affected in first order in u are expected to contribute only slightly on ac-

count of their smaller magnitudes in comparison with t and t_\perp .

Acknowledgments

V.M.P. is supported by Fundação para a Ciência e a Tecnologia (FCT) via SFRH/BPD/27182/2006, and acknowledges Centro de Física do Porto for computational support. N.M.R.P and V.M.P acknowledge the support of POCI 2010 via PTDC/FIS/64404/2006. R.M.R. acknowledges the support of FCT under the SeARCH (Services and Advanced Research Computing with HTC/HPC clusters) project (contract CONCREEQ/443/2005).

APPENDIX A: BANDSTRUCTURE PARAMETERS

With respect to the bandstructure depicted in Fig. 7, the notable momenta are ($\nu_F = 3ta/2$):

$$q_1 = \frac{1}{2\nu_F} \sqrt{\frac{V^4 + 2V^2 t_\perp^2}{t_\perp^2 + V^2}}, \quad (\text{A1a})$$

$$q_2 = \frac{V}{\nu_F}, \quad (\text{A1b})$$

$$q_3 = \frac{1}{\nu_F} \sqrt{V^2 + 2t_\perp^2}, \quad (\text{A1c})$$

while the corresponding energies are

$$E_1 = \frac{1}{2} \frac{t_\perp V}{\sqrt{V^2 + t_\perp^2}}, \quad (\text{A2a})$$

$$E_2 = \frac{V}{2}, \quad (\text{A2b})$$

$$E_3 = \frac{1}{2} \sqrt{V^2 + 4t_\perp^2}. \quad (\text{A2c})$$

The energy gap is given by

$$\Delta = 2E_1 = \frac{t_\perp V}{\sqrt{V^2 + t_\perp^2}}, \quad (\text{A3})$$

and the midpoint between the upper bands at $q = 0$ is at

$$E_{\text{mid}} = \frac{V + \sqrt{V^2 + 4t_\perp^2}}{4}, \quad (\text{A4})$$

to which corresponds the momentum

$$q_{E_{\text{mid}}} = \frac{1}{2\nu_F} \sqrt{V^2 + 4E_{\text{mid}} + 2\sqrt{4E_{\text{mid}}(t_\perp^2 + V^2) - t_\perp^2 V^2}}. \quad (\text{A5})$$

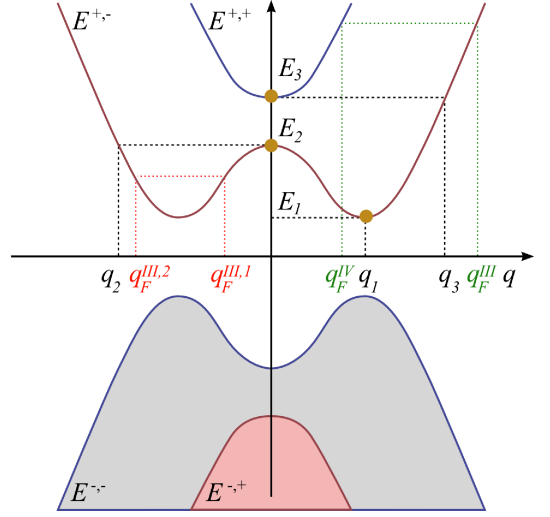


FIG. 7: (color online) Schematic representation of an arbitrary cut of the bandstructure of bilayer graphene close to the Dirac point.

APPENDIX B: ENERGY INTEGRALS

To compute the total electronic energy, the evaluation of the integral

$$F^{\pm,\pm} \equiv \pm \frac{1}{2} \int k dk \sqrt{A + Bk^2 \pm 2\sqrt{D + Ek^2}} \quad (\text{B1})$$

is required. The parameters, with respect to the dispersion of the bilayer in Eq. (6), are given as

$$A = V^2 + 2t_\perp^2, \quad B = 4\nu_F^2, \quad D = t_\perp^4, \\ E = 4\nu_F^2(tp^2 + V^2). \quad (\text{B2})$$

The integral is readily computed by changing to the variable $x \equiv \sqrt{D + Ek^2}$, after which it becomes

$$\int x dx \sqrt{\alpha + \beta x + \gamma x^2}, \quad (\text{B3})$$

and is readily available in standard tables. The final result is thus

$$F^{\eta_1, \eta_2} = \frac{\eta_1}{4\nu_F^2(t_\perp^2 + V^2)} \left\{ \frac{R^{3/2}}{3\gamma} - \frac{\gamma x + \eta_2}{2\gamma^2} \eta_2 \sqrt{R} \right. \\ \left. - \frac{\eta_2 \Delta}{8\gamma^{5/2}} \log \left(2\sqrt{\gamma R} + 2\gamma x + 2\eta_2 \right) \right\}, \quad (\text{B4})$$

where

$$\begin{aligned}
R &\equiv \alpha + \beta x + \gamma x^2, \\
\Delta &\equiv 4\alpha\gamma - \beta^2 = \frac{4V^2 t_\perp^2}{(t_\perp^2 + V^2)^2}, \\
\alpha &\equiv A - \frac{BD}{E} = \frac{V^4 + t_\perp^4 + 3t_\perp^2 V^2}{t_\perp^2 + V^2}, \\
x &\equiv \sqrt{t_\perp^4 + 4\nu_F^2(t_\perp^2 + V^2)k^2}, \\
\gamma &= \frac{1}{t_\perp^2 + V^2}, \\
\beta &= \pm 2.
\end{aligned} \tag{B5}$$

-
- ¹ A. H. Castro Neto, F. Guinea, N. M. R. Peres, K. S. Novoselov, and A. K. Geim, arXiv:0709.1163 (2007).
- ² K. S. Novoselov, A. K. Geim, S. V. Morozov, D. Jiang, Y. Zhang, S. V. Dubonos, I. V. Grigorieva, and A. A. Firsov, *Science* **306**, 666 (2004).
- ³ K. S. Novoselov, A. K. Geim, S. V. Morozov, D. Jiang, M. I. Katsnelson, I. V. Grigorieva, S. V. Dubonos, and A. A. Firsov, *Nature* **438**, 197 (2005).
- ⁴ K. S. Novoselov, D. Jiang, F. Schedin, T. J. Booth, V. V. Khotkevich, S. V. Morozov, and A. K. Geim, *Proc. Natl. Acad. Sci. USA* **102**, 10453 (2005).
- ⁵ A. H. Castro Neto, F. Guinea, and N. M. R. Peres, *Physics World* **19**, 33 (2006).
- ⁶ M. I. Katsnelson and K. S. Novoselov, *Solid State Commun.* **143**, 3 (2007).
- ⁷ S. V. Morozov, K. S. Novoselov, M. I. Katsnelson, F. Schedin, D. C. Elias, J. A. Jaszczak, and A. K. Geim, *Phys. Rev. Lett.* **100**, 016602 (2008).
- ⁸ K. S. Novoselov, E. McCann, S. V. Morozov, V. I. Fal'ko, M. I. Katsnelson, U. Zeitler, D. Jiang, F. Schedin, and A. K. Geim, *Nat. Phys.* **2**, 177 (2006).
- ⁹ T. Ohta, A. Bostwick, T. Seyller, K. Horn, and E. Rotenberg, *Science* **313**, 5789 (2006).
- ¹⁰ E. McCann, *Phys. Rev. B* **74**, 161403R (2006).
- ¹¹ E. V. Castro, K. S. Novoselov, S. V. Morozov, N. M. R. Peres, J. M. B. L. dos Santos, J. Nilsson, F. Guinea, A. K. Geim, and A. H. Castro Neto, *Phys. Rev. Lett.* **99**, 216802 (2007).
- ¹² J. B. Oostinga, H. B. Heersche, X. Liu, A. F. Morpurgo, and L. M. K. Vandersypen, *Nat. Mater.* **7**, 151 (2008).
- ¹³ W. P. Su, J. R. Schrieffer, and A. J. Heeger, *Phys. Rev. Lett.* **42**, 1698 (1979).
- ¹⁴ W. P. Su, J. R. Schrieffer, and A. J. Heeger, *Phys. Rev. B* **22**, 2099 (1980).
- ¹⁵ C. R. Fincher, D. L. Peebles, A. J. Heeger, M. A. Druy, Y. Matsumura, A. G. MacDiarmid, H. Shirakawa, and S. Ikeda, *Solid State Commun.* **27**, 489 (1978).
- ¹⁶ G. M. Rutter, J. N. Crain, N. P. Guisinger, T. Li, P. N. First, and J. A. Strosio, *Science* **317**, 219 (2007).
- ¹⁷ M. S. Dresselhaus and G. Dresselhaus, *Adv. Phys.* **51**, 1 (2002).
- ¹⁸ L. Wirtz and A. Rubio, *Solid State Commun.* **131**, 141 (2004).
- ¹⁹ H. J. F. Jansen and A. J. Freeman, *Phys. Rev. B* **35**, 8207 (1987).
- ²⁰ J. C. Boettger, *Phys. Rev. B* **55**, 11202 (1997).
- ²¹ N. Mounet and N. Marzari, *Phys. Rev. B* **71**, 205214 (2005).
- ²² R. J. Nemanich, G. Lucovsky, and S. A. Solin, *Mat. Sci. and Eng.* **31**, 157 (1977).
- ²³ J.-N. Fuchs and P. Lederer, *Phys. Rev. Lett.* **98**, 016803 (2007).
- ²⁴ J. C. Slater and G. F. Koster, *Phys. Rev.* **94**, 1498 (1954).
- ²⁵ W. A. Harrison, *Elementary Electronic Structure* (World Scientific, 1999).
- ²⁶ E.-A. Kim and A. H. Castro Neto, arXiv:cond-mat/0702562 (2007).
- ²⁷ D. A. Papaconstantopoulos, M. J. Mehl, S. C. Erwin, and M. R. Pederson, in *Tight-Binding Approach to Computational Materials Science*, edited by P. Turchi, A. Gonis, and L. Colombo (Materials Research Society, Pittsburgh, 1998), p. 221.
- ²⁸ T. Ohta, A. Bostwick, J. L. McChesney, T. Seyller, K. Horn, and E. Rotenberg, *Phys. Rev. Lett.* **98**, 206802 (2007).
- ²⁹ L. M. Malard, J. Nilsson, D. C. Elias, J. C. Brant, F. Plentz, E. S. Alves, A. H. C. Neto, and M. A. Pimenta, *Phys. Rev. B* **76**, 201401 (2007).
- ³⁰ J. Yan, E. A. Henriksen, P. Kim, and A. Pinczuk, arXiv:0712.3879 (2007).
- ³¹ M. Lazzeri, C. Attaccalite, L. Wirtz, and F. Mauri, *Phys. Rev. B* **78**, 081406 (2008).
- ³² H. J. Monkhorst and J. D. Pack, *Phys. Rev. B* **13**, 5188 (1968).
- ³³ C. Hartwigsen, S. Goedecker, and J. Hutter, *Phys. Rev. B* **58**, 3641 (1998).